Nanotechnology

PAPER

Multiband and broadband active controllable terahertz absorption in dual-side grating-gate graphene field-effect transistors

To cite this article: Anqi Yu *et al* 2020 *Nanotechnology* **31** 284001

IOP Publishing Nanotechnology

Nanotechnology **31** (2020) 284001 (7pp) https://doi.org/10.1088/1361-6528/ab86ed

Multiband and broadband active controllable terahertz absorption in dual-side grating-gate graphene field-effect transistors

Anqi Yu[1,2], Xuguang Guo[1,2], Alexei V Balakin[1,3,4], Alexander P Shkurinov[1,3,4] and YiMing Zhu[1,2]

[1] Shanghai Key Lab of Modern Optical System, Terahertz Technology Innovation Research Institute, Terahertz Spectrum and Imaging Technology Cooperative Innovation Center, University of Shanghai for Science and Technology, 516 Jungong Road, Shanghai 200093, People's Republic of China
[2] Shanghai Institute of Intelligent Science and Technology, Tongji University, Shanghai, People's Republic of China
[3] Faculty of Physics and International laser Center, Lomonosov Moscow State University, Leninskie Gory 1–2, Moscow 19991, Russia
[4] ILIT RAS – Branch of the FSRC 'Crystallography and Photonics' RAS, Svyatoozerskaya 1, 140700, Shatura, Moscow Region, Russia

E-mail: xgguo@usst.edu.cn and ymzhu@usst.edu.cn

Received 27 December 2019, revised 20 March 2020
Accepted for publication 6 April 2020
Published 28 April 2020

Abstract

We show that the even order ungated modes can be excited under normal incidence while the odd order ungated modes cannot in traditional single-side grating-gate graphene field-effect transistors. The odd order ungated modes will suppress the excitation efficiency of the gated modes. In order to realize multiband detection by effectively exciting the higher order gated modes, the frequency of the 1st order ungated mode should be tuned up, which can be realized by shortening the length of the ungated region. We propose to use the dual-side grating-gate structure to shorten the length of the ungated region. Gated mode up to 21st order can be realized in complementary dual-side grating-gate structure. The ultra-multiband absorption can be actively controlled to cover 1.06–10 THz when the graphene Fermi energy is tuned from 0.2 eV to 0.6 eV. Even order gated modes will be excited by gradually overlapping the two grating layers because of the break of symmetry. Broadband detection from 0.1–8.2 THz can be realized by the effective excitation and overlap of the odd and even order gated modes.

Keywords: graphene, plasmon, terahertz detector

(Some figures may appear in colour only in the online journal)

1. Introduction

The optoelectronic technologies have been well developed in the past few decades. However, the so called 'terahertz (THz) gap', which consists of the electromagnetic waves with frequencies ranging from 0.1 THz to 10 THz, is yet to be covered. Currently, commercial THz devices either lack tunability or need to work in cryogenic environment [1, 2], limiting their practical applications. Surface plasmons, the collective oscillation of charge carriers is promising to solve the problems. Once excited by the spatial electromagnetic waves, plasmons can help to confine the energy of the incident waves at the vicinity of the insulator/conductor interface [3–6]. Since the proposal by Dyakonov and Shur of directly detecting THz waves by generating plasmon-induced photocurrent [7], researchers began to study such self-rectified photocurrent in single gate MOSFET devices [8–10]. Later researchers began to study grating-gate MOSFET devices [11–24].

Two kinds of plasmon modes, referred to as gated modes and ungated modes, can be excited in channel regions right below the gratings (gated region) and the openings (ungated region), respectively. The plasmon drag effect and the plasmon ratchet effect, which can be utilized to detect the THz waves, were theoretically predicted and their responsivities were calculated [10, 22, 23]. Record response of 22.7 kV W^{-1} at 0.2 THz was experimentally demonstrated and attributed to the plasmon ratchet effect [20]. Despite the great success achieved in III–V grating-gate MOSFET detectors, the performances of these devices are greatly influenced at room temperature [12]. the theoretical calculations show that the responsivity of the two effects are related with the scattering rate [23]. As a kind of two-dimensional material with Dirac energy band, the scattering rate is predicted to be on the order of picosecond for high-quality graphene (mobility $> 2 \times 10^5 cm^2$ V s^{-1}). Therefore, high-quality graphene-based grating-gate MOSFET detectors are promising to yield higher responsivity.

One of the advantages of semiconductors/semimetals plasmons is the post-fabrication tunability: as plasmons' dispersion is related to the carrier density, the frequency of a resonance mode excited in semiconductors/semimetals can be easily changed by tuning the carrier density with an applied gate voltage. However, the post-fabrication tunability cannot promise to cover the whole THz region with a single resonance mode. For III–V materials and graphene, the plasmon angular frequency $\omega_{sp} \propto n^{1/2}$ [13–17] and $\omega_{sp} \propto n^{1/4}$ [25, 26], respectively. Therefore, it is difficult to tune the frequency of a resonance mode, e.g. from 1 THz to 3 THz, because of the breakdown. As a result, graphene fermi energy can only be tuned within a limited range. In order to cover as broad frequency range as possible with only one device, strong multiple resonance modes are required. Unfortunately, the excitation efficiencies of the resonance modes are related with the net dipole moment [27]. Therefore, the excitation efficiencies of the lower order modes are always higher than those of the higher order modes. Thus, it is difficult to realize simultaneous near-critical coupling for multiple resonance modes.

In this work, we show that even order modes in the ungated region can be excited by normal incidence (referred to as ungated bright modes) while odd order modes cannot (referred to as ungated dark modes). If the frequency of a gated mode is close to that of an ungated dark mode, the excitation efficiency of the gated mode will be suppressed by the ungated dark mode. In order to achieve multiband absorption by efficiently exciting the higher order gated modes, such suppression should be avoided. Then the frequencies of the gated modes should be lower than that of the 1st order ungated dark mode. We propose to use dual-side grating-gates to increase the frequency of the 1st order ungated dark mode, thus the gated modes within the 1st order ungated dark mode will be enhanced and their absorption rates are nearly the same. We further show that the even order gated modes will be excited by overlapping the top and bottom grating-gates because of the break of symmetry. Broadband absorption can be realized by appropriately overlapping the grating-gates. The proposed structure may be applied as active controllable multiband or broadband THz detectors, sensors and switches.

2. Traditional single-side grating-gate structure

Figure 1(a) schematically shows the simulated traditional grating-gate structure. The simulation is performed by the finite-difference-time-domain method. The metal is modeled as perfect electric conductor. Because the refractive indices of many dielectrics are nearly constant in the THz frequencies [28], the refractive indices of the barrier layer and the substrate are assumed to be constant 1.7. The thickness of the barrier layer is $h = 40$ nm. Graphene conductivity is modeled by the Kubo formula [29]. The scattering rate γ throughout the full text is calculated by $1/\gamma = \mu E_F/ev_F^2$, with μ the graphene mobility, E_F the graphene Fermi energy, e the electron charge, and $v_F = 10^8$ cm s^{-1} the graphene Fermi velocity. In this section, μ is assumed to be 10000 cm^2 V s^{-1} and E_F is assumed to be 0.8 eV. Although the experimental results show that μ varies with E_F [30–34], the relationship between μ and E_F varies with the substrate because the dominating scattering mechanism are different for graphene on different substrates [35]. Therefore, μ is assumed to be irrelevant of E_F for simplicity.

Gated modes and ungated modes were once considered as plasmon modes localized in the gated regions and the ungated regions, respectively. However, as plasmons can be considered as in-plane electromagnetic waves, the lateral periodic alternation of the gated/ungated regions should be considered as lateral one-dimensional plasmonic crystal [36–38]. Therefore, the gated regions and the ungated regions are actually conductively connected with each other. The gated modes are influenced by the ungated regions and vice versa. Popov *et al* noticed that the gated modes become weaker when the electron density in the ungated region tends to zero, which demonstrates that the ungated region plays an important role in the excitation of the gated modes [13]. In the following, we show the importance of the ungated region to the excitation of the gated modes from another perspective.

As the plasmon modes excited in the grating-gate structure are considered as electromagnetic waves in the lateral one-dimensional plasmonic crystal, the dispersion relation under zero source-drain bias can be calculated as [37, 38]

$$\cos(\theta) = \cos(k_g W)\cos(k_u S) - Z \times \sin(k_g W)\sin(k_u S) \quad (1)$$

$$Z = 1 - 2\frac{r_+ r_-}{t_+ t_-} \quad (2)$$

where θ is the Bloch wavevector. k_g and k_u are the wavevectors in the gated and ungated regions, respectively. W and S are the lengths of the gated and ungated regions, respectively. r_+, r_-, t_+, t_- are the reflection and transmission coefficients at the ungated/gated boundary. It can be seen from equation (1) that a resonance mode is excited when $k_g W$ or $k_u S$ is close to $n\pi$. Since k_g is larger than k_u [11, 39], for the ungated modes, the electric field at the gated/ungated boundary in the ungated region is close to anti-node. Therefore, even order modes ($n = 2, 4, 6\ldots$) can be excited under normal incidence while odd order modes ($n = 1, 3, 5\ldots$) cannot for the ungated modes. On the contrary, for the gated modes, odd order modes can be excited while even order modes cannot.

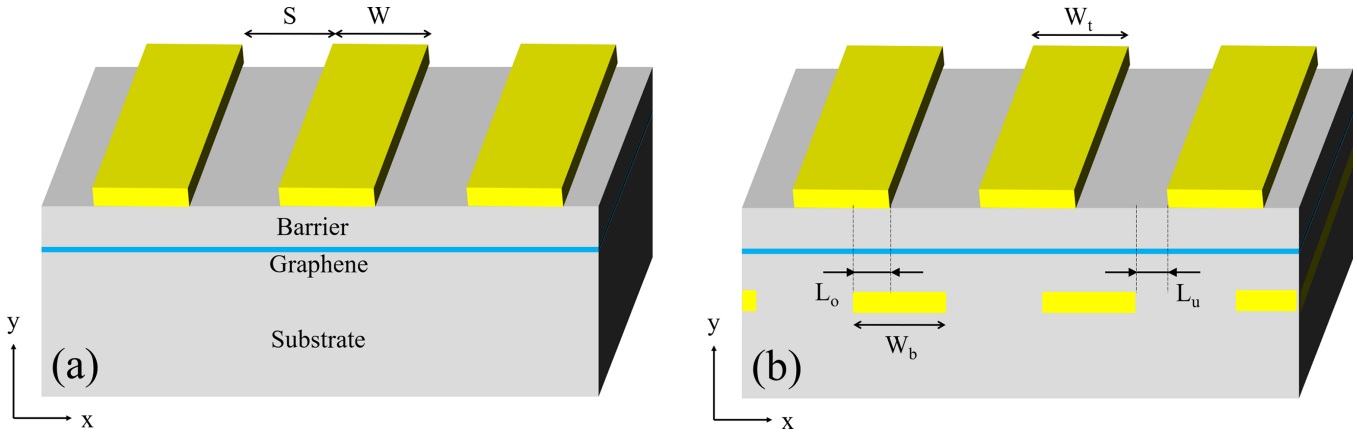

Figure 1. (a) The traditional single-side grating-gate structure. (b) The proposed dual-side grating-gate structure.

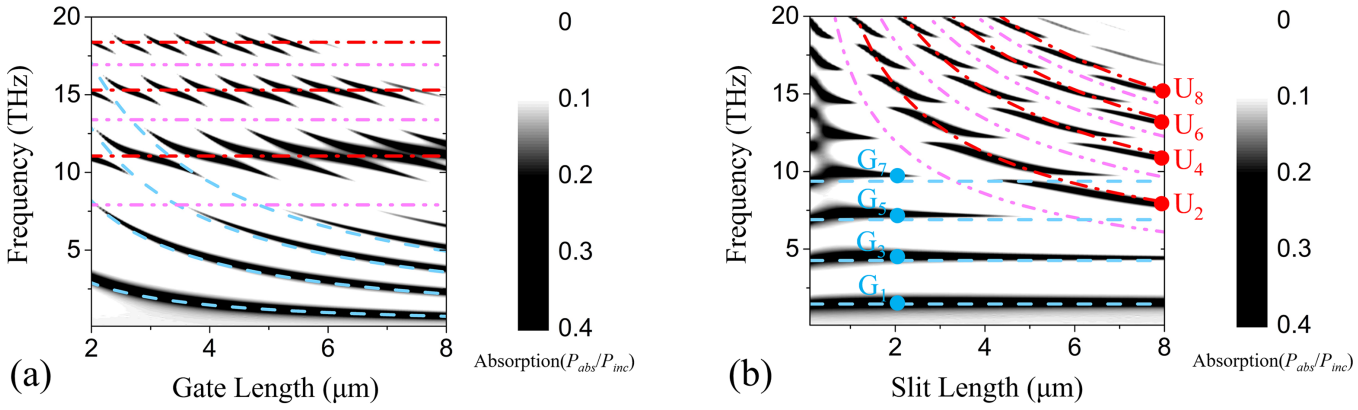

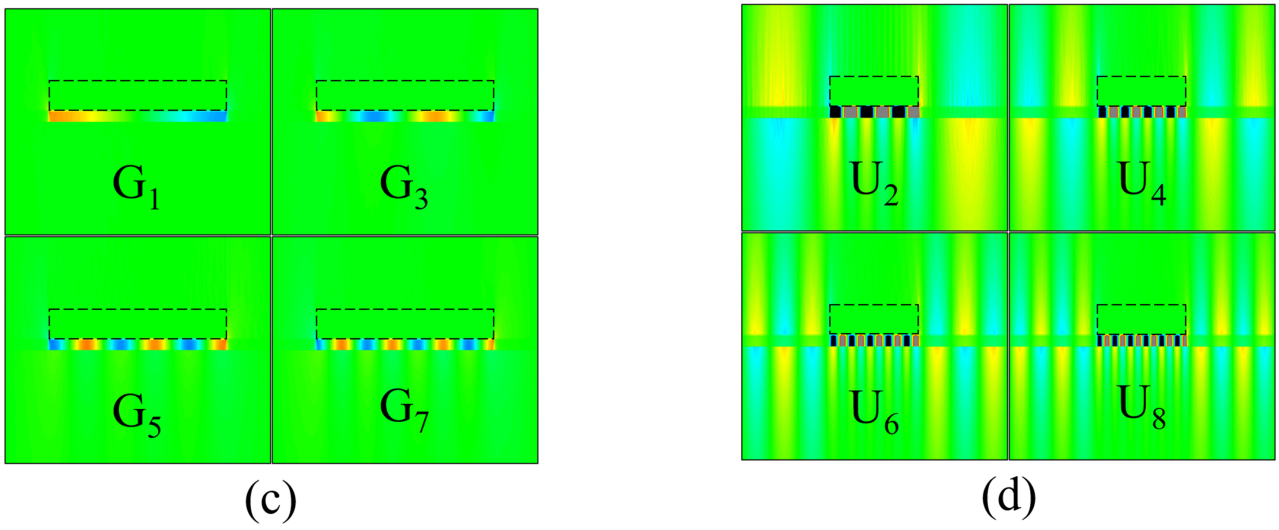

Figure 2. (a) The absorption contour of the single-side grating-gate structure as a function of *W*. P_{abs} and P_{inc} represent absorbed power and incident power, respectively. (b) The absorption contour of the single-side grating-gate structure as a function of *S*. The blue dashed lines represent the gated odd order modes, the red dash-dotted lines represent the ungated even order modes and the pink dash-dot-dotted lines represent the ungated odd order modes. (c) The Re(E_y) distributions corresponding to G_1, G_3, G_5 and G_7 as given in (b). (d) The Re(E_y) distributions corresponding to U_2, U_4, U_6 and U_8 as given in (b). The black dashed rectangles indicate the gates.

Figure 2(a) shows the contour plot of the resonance absorption as the gate length W is increased from 2 μm to 8 μm and the length S of the opening is fixed at 4 μm. The blue dashed curves are calculated by [25]

$$\omega = \sqrt{\frac{e^2 E_F k_{g,u}}{2\pi\hbar^2\varepsilon_0\varepsilon^*}} \tag{3}$$

where $k_{g,u}$ stands for either $k_g = n\pi/W$ (n = 1, 3, 5, 7) or k_u, $\hbar$ is the reduced Plank constant, ε_0 is the vacuum dielectric constant and ε^* is the effective relative dielectric constant calculated by equation (4) [11, 13, 14].

$$\varepsilon^* = \frac{1}{2}\left[\varepsilon_s + \varepsilon_b \coth(k_g W)\right] \tag{4}$$

The red dash-dotted lines are calculated by equation (3) and [11]

$$\varepsilon^* = \frac{1}{2}\left[\varepsilon_s + \varepsilon_b \frac{1 + \varepsilon_b \tanh(k_u S)}{\varepsilon_b + \tanh(k_u S)}\right] \tag{5}$$

with $k_u = n\pi/S_{eff}$ (n = 2, 4, 6, 8). Because of the existence of the metallic gratings, the effective dielectric constant is larger than that calculated by equation (5) and then the real k_u is larger than that calculated by equation (5). Therefore, an effective length $S_{eff} = 3.3$ μm is used as the denominator instead of $S = 4$ μm in calculating k_u to get a larger k_u. Obviously, the blue dashed lines correspond well with the simulated gated modes, which are proved to be 1st, 3rd, 5th and 7th order gated modes by the Re(E_y) distributions shown in figure 2(c). The red dash-dotted lines, however, do not seem to correspond with the simulated ungated modes as a result of the frequent anti-crossing between the gated modes and ungated modes. U_2, U_4, U_6 and U_8 are chosen as absorption peaks away from the anti-crossing regions, where the red dash-dotted lines correspond with the absorption peaks. The Re(E_y) distributions of U_2, U_4, U_6 and U_8 show that they are 2nd, 4th, 6th and 8th order ungated modes. Thus, the simulation results demonstrate the above analysis: even order ungated modes are excited.

Here it should be noted that all the gated modes will gradually become weak and finally disappear around the pink dash-dot-dotted lines. The pink curves are calculated by equations (3) and (5) with $k_u = n\pi/S_{eff}$ (n = 1, 3, 5, 7). Figure 2(b) shows the contour plot of the resonance absorption as S is increased from 0.2 μm to 8 μm and W is fixed at 4 μm. Similarly, the gated modes disappear around the ungated dark modes. Then It can be inferred that the gated modes will be suppressed at the vicinity of the ungated dark modes, further implying an important role that the ungated region plays on the excitation of the gated modes.

3. Dual-side grating-gate structure

According to the results shown above, the frequency of the 1st order ungated dark mode should be higher than 10 THz so that the excitation efficiencies of the higher order gated modes within 10 THz will not be suppressed by it. Popov *et al* showed the efficient excitation of the gated mode up to the 11th order by reducing the slit length in single-side grating-gate structures [11, 13]. Experimentally, reducing the slit length to sub-100 nm will bring difficulties in the lift off process. To avoid such experimental difficulties, we propose to use dual-side grating-gate structure, as shown in figure 1(b). If the openings of the top gratings and the gates of the bottom gratings are aligned, the ungated region is nearly physically eliminated. Here the barrier thickness is reduced to 20 nm. The mobility of graphene is assumed to be 40000 cm^2 V s^{-1} in order to clearly show the gradual excitation of the even order gated modes, which will be discussed later. Because of the slight difference in the effective dielectric environment between the top-gated and bottom-gated regions, the top gate length W_t and the bottom gate length W_b are set as 6 μm and 6.15 μm, respectively.

The top and bottom gates are initially assumed to be completely complementary, that is, the lengths L_o of the overlapping regions and the lengths L_u of the ungated regions are both 0 μm. Figure 3(a) shows the absorption spectra of the proposed structure. It is seen that the absorption peaks with absorption exceeding 30% cover the frequency range from 1.06–10 THz when the graphene Fermi energy is increased from 0.2 eV to 0.6 eV. The $Re(E_y)$ distributions given in figure 3(b) show that the gated modes from the 1st order to the 21st order are excited. It should be mentioned that the absorption at resonance can be calculated by [15, 21]

$$A = \frac{2\gamma_{rad}\gamma_{dis}}{(\gamma_{rad} + \gamma_{dis})^2}\left(1 - \sqrt{R_0}\right) \tag{6}$$

for such no-reflector structure, where A stands for absorption, γ_{rad} for the radiative damping, $\gamma_{dis} = \gamma$ for the scattering rate, R_0 for the reflection at the air/substrate interface. Then the maximum absorption for $n = 1.7$ is about 37%, which is achieved by the absorption peaks. The efficient excitation of gated mode up to the 21st order should be attributed to the shrinkage of the ungated region.

Although the even order gated modes cannot be excited under normal incidence in single-side grating-gate structures, they may be excited once the symmetry is broken. The break of symmetry can be achieved by oblique incidence or by creating structural asymmetry. Todorov *et al* reported the excitation of even order localized surface plasmon modes by oblique incidence [27]. In the following, we show that the even order gated modes can be excited by structural asymmetry. As seen in figure 4(a), more absorption peaks will be gradually excited from higher frequencies to lower frequencies when the bottom gates are gradually translated leftward. The Re(E_y) distributions as given in figure 4(b) show that peaks I, II and III are 2nd, 4th and 6th order gated modes. Then it can be concluded that these new resonance modes are the even order gated modes. In the top gated region, the effective dielectric constant in the overlapping region is larger than that in the non-overlapping region, so that the symmetry in the dielectric environment is broken by the structure and the net dipole moment of the even order gated modes are not 0. The smallest value of L_o for the efficient excitation of a '2nth' order gated mode can be roughly estimated as follows. According to equation (4), the effective dielectric constant in the overlapping region is about $2^{1/2}$ times that in the non-overlapping region. Assuming that the efficient excitation of a '2nth' order gated mode requires nodes at the boundary of the overlapping region, the smallest value of L_o can be calculated as

$$L_o^{2n} = \frac{1/\sqrt{2}}{1/\sqrt{2} + 2n - 1} \times W_t \tag{7}$$

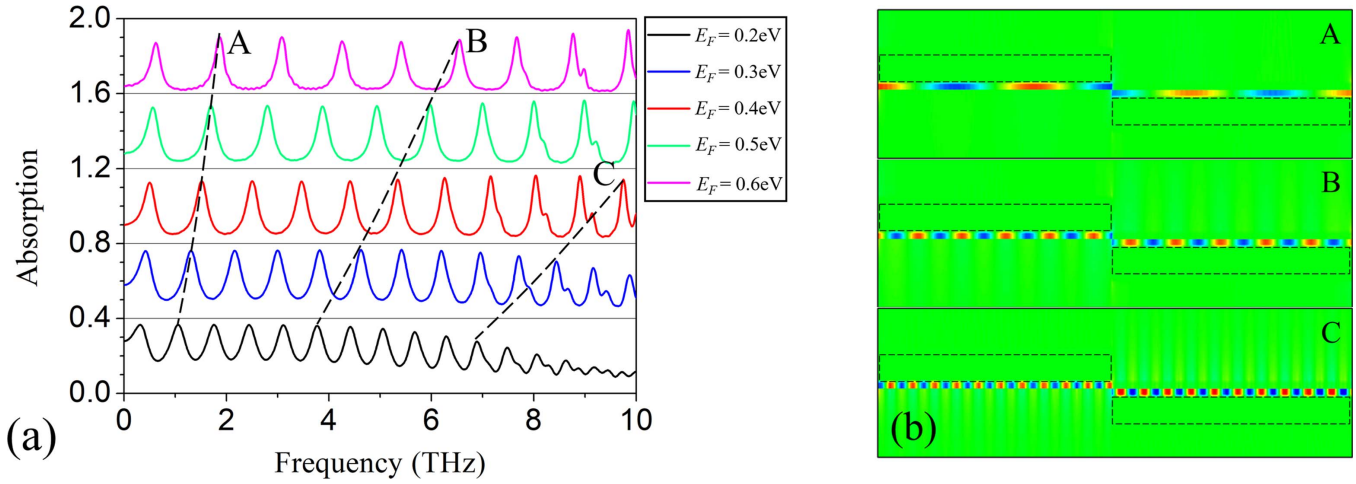

Figure 3. (a) The absorption spectra of the dual-side grating-gate structure with E_F tuned from 0.2 eV to 0.6 eV. (b) $Re(E_y)$ distributions corresponding to peaks A, B and C. The black dashed rectangles indicate the gates.

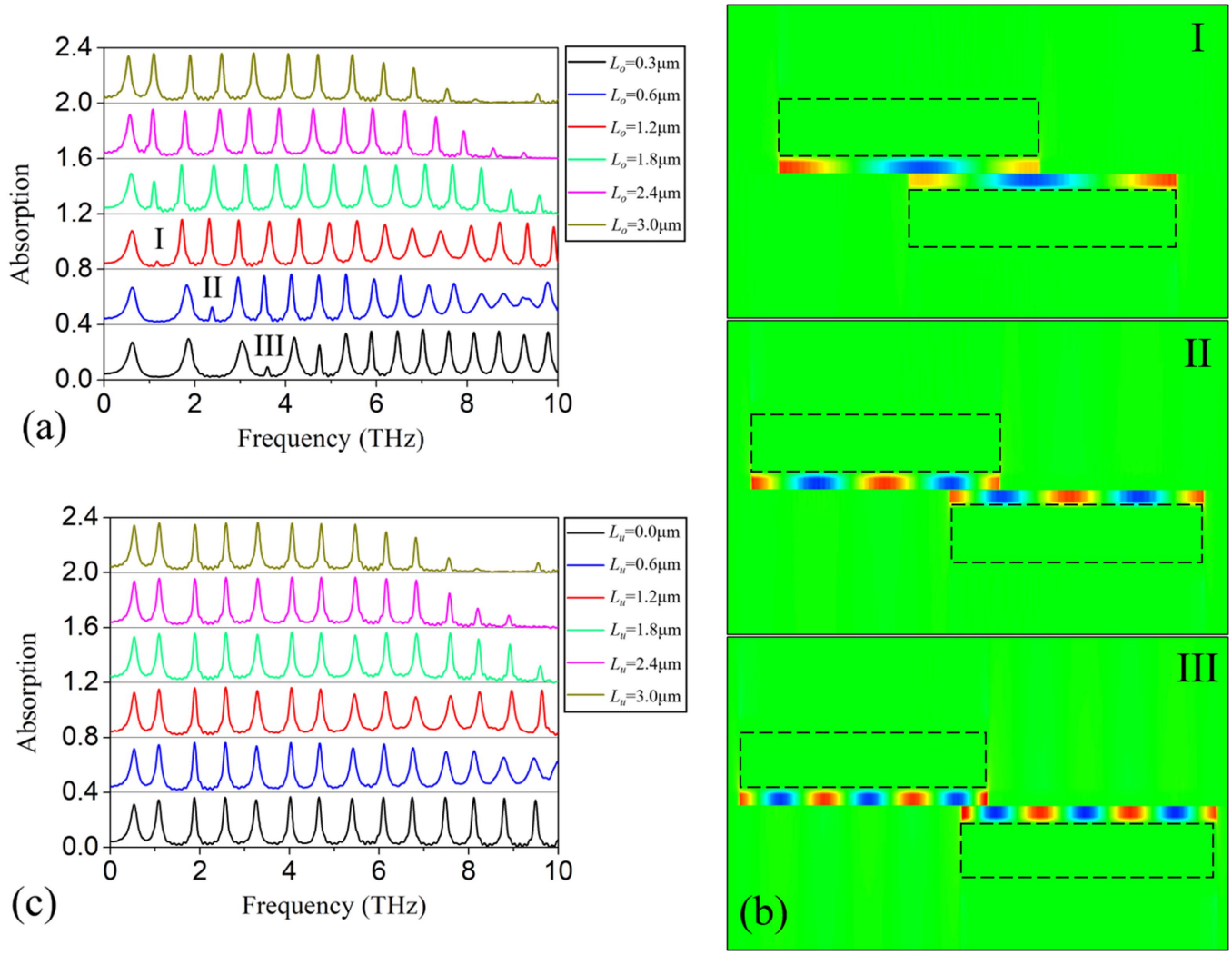

Figure 4. (a) The absorption spectra of the dual-side grating-gate structure with L_o increased from 0 μm to 3 μm and the period length fixed at 12.15 μm. (b) The $Re(E_y)$ distributions corresponding to peaks I, II and III. (c) The absorption spectra of the dual-side grating-gate structure with L_o fixed at 3 μm and L_u changed from 0 μm to 3 μm. Here the graphene Fermi energy is $E_F = 0.4$ eV.

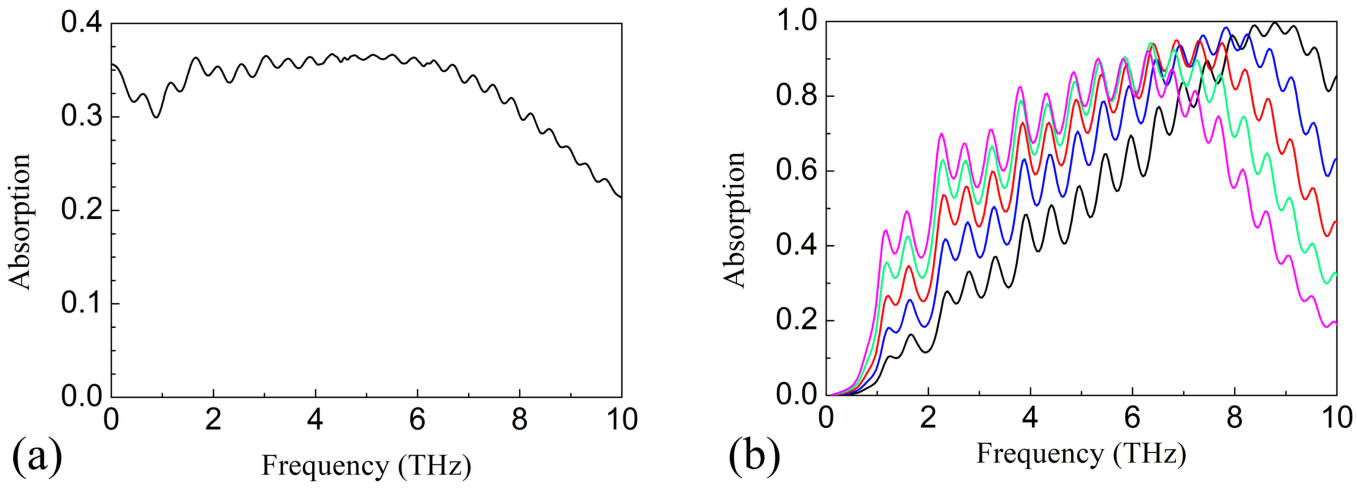

Figure 5. (a) The absorption spectra of the overlapping dual-side grating-gate structure with parameters: $W_t = 2.4$ μm, $W_b = 2.5$ μm, $L_o = 0.8$ μm, $L_u = 0.1$ μm, $h = 10$ nm, $E_F = 0.1$ eV. (b) The absorption spectra of the overlapping dual-side grating-gate structure with parameters: $W_t = 1.9$ μm, $W_b = 2.0$ μm, $L_o = 0.7$ μm, $L_u = 0.1$ μm, $h = 10$ nm, $E_F = 0.1$ eV. The separation between graphene and the metal reflector are 3 μm (black), 4 μm (blue), 5 μm (red), 6 μm (green) and 7 μm (magenta).

which yields $L_o = 2.49$ μm, 1.14 μm, 0.74 μm and 0.55 μm for the 2nd, 4th, 6th and 8th order modes, corresponding to figure 4(a). Therefore, the efficient excitation of a lower even order gated mode requires longer L_o. If L_o is gradually increased and the length of a period is kept fixed, however, L_u will increase accordingly. Then frequency of the 1st order ungated dark mode will redshift, finally suppressing the excitation efficiency of the higher order gated modes, as shown by the pink and yellow curves around 10 THz and 9 THz, respectively, as shown in figure 4(a). To avoid such suppression of the ungated dark mode, L_u should be reduced. Figure 4(c) shows that all the resonance modes within 10 THz will not be bothered when L_u is no longer than 1.2 μm.

Since plasmon resonances exhibit Lorentz-shape absorptions, they do not seem to meet the requirement for broadband purposes, which are usually realized by thermal-type or photon-type focal plane array. Recently Bai *et al* realized GaAs-based photon-type THz response covering 4.2–20 THz by the up-conversion technique [40]. However, thermal-type detectors often suffer from a tradeoff between speed and sensitivity, while photon-type detectors need cryogenic environment. In recent years, plasmonic THz broadband detection have been demonstrated by the overlap of two or more resonance modes [29, 41–44], which cover a limited frequency range within the THz frequencies. In this work, the efficient excitation of both the odd and even order gated modes in the THz range opens the possibility of plasmonic broadband detection over the whole THz frequencies: as the efficient excitation of the high order gated modes and the even order modes have been demonstrated possible, their overlapping with each other can possibly cover the entire THz range. As shown in figure 5(a), broadband absorption of more than 30% over 0.1–8.2 THz range can be achieved. By putting a metal reflector below the graphene layer, the absorption can be enhanced to more than 50% with bandwidth exceeding 6 THz as shown in figure 5(b). In our previous study [45], it was found that complete absorption is achieved when the reflection from the device surface and that from the metal reflector interfere destructively with each other. The requirement can be simultaneously met for several absorption peaks occasionally, such as the peaks around 8.8 THz of the black curve in figure 5(b) and those shown in [42–44, 46]. For the combination of about 20 absorption peaks, however, the requirement is too difficult to meet. Therefore, near-complete absorption (>90%) can only be achieved within a limited frequency range in the proposed structure.

4. Conclusions

In conclusion, we show that the ungated dark modes will suppress the excitation efficiency of the gated modes. The effective excitation of higher order gated modes can be achieved by up-tuning the frequency of the 1st ungated dark mode, which can be achieved by reducing the length of the slit between the metallic gates. We propose to use the complementary dual-side grating-gate structure to reduce the slit length to avoid the experimental difficulty in the lift off process. The efficient excitation up to the 21st order gated mode can be achieved. 1.06–10 THz can be covered by changing the graphene Fermi energy from 0.2 eV to 0.6 eV. Even order gated modes will be excited in the proposed structure when $L_o \neq 0$ μm because of the break of symmetry, leading to ultra-multiband THz detection. Broadband detection with absorption larger than 30% from 0.1–8.2 THz can be realized by appropriately overlapping the top and bottom gates with a short ungated region. The insertion of a metal reflector can help to enhance the absorption to more than 50% with bandwidth exceeding 6 THz. The proposed structure may find applications in actively tunable multiband or broadband THz detectors, sensors and switches.

Acknowledgments

This work was supported in part by the National Key Research and Development Program of China (2017YFA0701005), in

part by the National Natural Science Foundation of China (61722111, 61731020), the 111 Project (D18014), the International Joint Lab Program supported by Science and Technology Commission Shanghai Municipality (17590750300), in part by the Ministry of Science and Higher Education (075-15-2019-1950) and in part by the State assignment FSRC Crystallography and Photonics RAS.

ORCID iDs

Anqi Yu https://orcid.org/0000-0003-4615-8025
Xuguang Guo https://orcid.org/0000-0003-1733-6478

References

[1] Karasik B S and Cantor R 2011 *Appl. Phys. Lett.* **98** 193503
[2] Hayton D J, Gao J R, Kooi J W, Ren Y, Zhang W and de Lange G 2012 *Appl. Phys. Lett.* **100** 081102
[3] Wu Y, Niu J, Danesh M, Liu J, Chen Y, Ke L, Qiu C and Yang H 2016 *Appl. Phys. Lett.* **109** 041106
[4] Zhang L, Tang L, Wei W, Cheng X, Wang W and Zhang H 2016 *Opt. Express* **24** 20002
[5] Liu B, Tang C, Chen J, Wang Q, Pei M and Tang H 2017 *Opt. Express* **25** 12061
[6] Fang J, Wang D, Devault C T, Chung T F, Chen Y P, Boltasseva A, Shalaev V M and Kildishev A V 2017 *Nano Lett.* **17** 57
[7] Dyakonov M I and Shur M S 1996 *IEEE Trans. Electron Dev.* **43** 1640
[8] Knap W, Deng Y, Rumyantsev S, J-q L, Shur M S, Saylor C A and Brunel L C 2002 *Appl. Phys. Lett.* **80** 3433
[9] Shaner E A, Lee M, Wanke M C, Grine A D, Reno J L and Allen S J 2005 *Appl. Phys. Lett.* **87** 193507
[10] Aizin G R, Popov V V and Polischuk O V 2006 *Appl. Phys. Lett.* **89** 143512
[11] Popov V V 2011 *J. Infrared Milli. Terahz. Waves* **32** 1178
[12] Muravjov A V, Veksler D B, Popov V V, Polischuk O V, Pala N, Hu X, Gaska R, Saxena H, Peale R E and Shur M S 2010 *Appl. Phys. Lett.* **96** 042105
[13] Popov V V, Shur M S, Tsymbalov G M and Fateev D V 2007 *Int. J. High Speed Electron. Syst.* **17** 557
[14] Wang L, Chen X, Hu W, Yu A and Lu W 2013 *Appl. Phys. Lett.* **102** 243507
[15] Popov V V, Polischuk O V, Teperik T V, Peralta X G, Allen S J, Horing N J M and Wanke M C 2003 *J. Appl. Phys.* **94** 3556
[16] Popov V V, Fateev D V, Ivchenko E L and Ganichev S D 2015 *Phys. Rev.* B **91** 235436
[17] Popov V V, Fateev D V, Otsuji T, Meziani Y M, Coquillat D and Knap W 2011 *Appl. Phys. Lett.* **99** 243504
[18] Wang L, Hu W, Wang J, Wang X, Wang S, Chen X and Lu W 2012 *Appl. Phys. Lett.* **100** 123501
[19] Aizin G R, Fateev D V, Tsymbalov G M and Popov V V 2007 *Appl. Phys. Lett.* **91** 163507
[20] Jurita Y *et al* 2014 *Appl. Phys. Lett.* **104** 251114
[21] Popov V V, Fateev D V, Polischuk O V and Shur M S 2010 *Opt. Express* **18** 16771
[22] Fateev D V, Mashinsky K V and Popov V V 2017 *Appl. Phys. Lett.* **110** 061106
[23] Popov V V 2013 *Appl. Phys. Lett.* **102** 253504
[24] Karabiyik M, Ahmadivand A, Sinha R, Al-Amin C, Vabbina P K, Kaya S, Rupper G, Rudin S, Shur M and Pala N 2016 *Phys. Status Solidi* B **253** 671
[25] Jablan M, Buljan H and Soljačić M 2009 *Phys. Rev.* B **80** 245435
[26] Popov V V, Bagaeva T Y, Otsuji T and Ryzhii V 2010 *Phys. Rev.* B **81** 073404
[27] Todorov Y, Tosetto L, Teissier J, Andrews A M, Klang P, Colombelli R, Sagnes I, Strasser G and Sirtori C 2010 *Opt. Express* **18** 13886
[28] Palik E D 1998 *Handbook of Optical Constants of Solids* (San Diego: Academic Publisher)
[29] Cai Y and Xu K-D 2018 *Opt. Express* **26** 31693
[30] Banszerus L, Schmitz M, Engels S, Dauber J, Oellers M, Haupt F, Watanabe K, Taniguchi T, Beschoten B and Stampfer C 2015 *Sci. Adv.* **1** e1500222
[31] Lyon T J, Sichau J, Dorn A, Zurutuza A, Pesquera A, Centeno A and Blick R H 2017 *Appl. Phys. Lett.* **110** 113502
[32] Yan Z, Lin J, Peng Z, Sun Z, Zhu Y, Li L, Xiang C, Samuel E L, Kittrell C and Tour J M 2012 *ACS Nano* **6** 9110
[33] Wang L *et al* 2013 *Science* **342** 614
[34] Brown M A, Crosser M S, Leyden M R, Qi Y and Minot E D 2016 *Appl. Phys. Lett.* **109** 093104
[35] Hirai H, Tsuchiya H, Kamakura Y, Mori N and Ogawa M 2014 *J. Appl. Phys.* **116** 083703
[36] Sydoruk O, Wu J B, Mayorov A, Wood C D, Mistry D K and Cunningham J E 2015 *Phys. Rev.* B **92** 195304
[37] Petrov A S, Svintsov D, Ryzhii V and Shur M S 2017 *Phys. Rev.* B **95** 045405
[38] Yu A 2018 *J. Phys. D: Appl. Phys.* **51** 395103
[39] Eguiluz A, Lee T K and Quinn J J 1975 *Phys. Rev.* B **11** 4989
[40] Bai P *et al* 2019 *Nat. Commun.* **10** 3513
[41] Xia S-X, Zhai X, Wang L-L and Wen S-C 2020 *Opt. Lett.* **45** 93
[42] Gao F, Zhu Z, Xu W, Zhang J, Guo C, Liu K, Yuan X and Qin S 2017 *Opt. Express* **25** 9579
[43] Ye L, Chen Y, Cai G, Liu N, Zhu J, Song Z and Liu Q H 2017 *Opt. Express* **25** 11223
[44] Yang J, Zhu Z, Zhang J, Guo C, Xu W, Liu K, Yuan X and Qin S 2018 *Sci. Rep.* **8** 3239
[45] Yu A 2018 *Superlattices Microstruct.* **122** 461
[46] Xia S-X, Zhai X, Huang Y, Liu J-Q, Wang L-L and Wen S-C 2017 *Opt. Lett.* **42** 3052